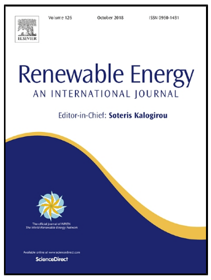

A parameter study and optimization of two body wave energy converters

Elie Al Shami, Xu Wang, Ran Zhang, Lei Zuo

PII: S0960-1481(18)30783-3

DOI: 10.1016/j.renene.2018.06.117

Reference: RENE 10273

To appear in: *Renewable Energy*

Received Date: 11 January 2018

Accepted Date: 30 June 2018

A parameter study and optimization of two body wave energy converters

Elie Al Shami[a], Xu Wang[a*], Ran Zhang[a], Lei Zuo[b]

[a*]School of Engineering, RMIT University, Australia

Telephone: 03 9925 6028

Fax: 03 9925 6108

Email: xu.wang@rmit.edu.au

[b]Department of Mechanical Engineering, Virginia Polytechnic Institute and State University, USA

Abstract

This paper studies the multidisciplinary nature of two body wave energy converters by a parametric study based on the Taguchi method which helps to understand the effect of different dependent parameters on the wave energy conversion performance. Seven different parameters are analyzed and their effect on the maximum captured power, resonance frequency and bandwidth is studied. An interesting comparison between a cylindrical submerged body and a spherical one was made in terms of the system's viscous damping and hydrodynamics. The best system parameter combinations based on the maximum output power, best resonant frequency and frequency bandwidth were identified from the outcomes of the Taguchi method and optimized to capture the maximum power to operate in the specific (Australian) sea regions where the waves' frequencies are relatively low. This paper should provide a guideline for designers to tune their parameters based on the desired performance and sea state.

Keywords: parameter, optimization, two body wave energy converters, power, bandwidth, Taguchi method

1. Introduction

Renewable energy has been established as one of the most prolific development areas in the twenty first century. The difficulties surrounding exploiting renewable energy resources are no longer related to developing novel technologies, but rather related to the transition and implementation of the renewable harvesting systems within the petrol based power grids around the world.

Solar energy, hydropower and wind energy are all being harvested by technologies which are witnessing a high rise in usage, and have been well established and optimized within industry manufacturers. Ocean energy conversion technology on the other hand, while it has a potentially higher efficiency and reduced complexity, is struggling to find its place in the renewable energy market.

There are three main types of WECs: point absorbers, terminators, and attenuators, and many modes of operation [1]. These devices have undergone much research and development since there were more than 1000 WEC devices in 2009. With such large amount of research and development, one must attribute the difficulties of the wave energy converter development to the multidisciplinary nature of harvesting power from ocean waves. For example, hydropower is highly accounted for fluid and thermo dynamics, this results in a convergence and simplicity of the focus on developing hydropower energy harvesters. On the other hand, as presented in [2], wave energy harvesters are related to many disciplines and factors, as their performance is highly affected by the PTO (power take-off) system, the hydrodynamic design, and dynamics and control in an attempt to increase the WEC efficiency for different sea states.

This multidisciplinary nature results in difficulties to optimize WECs, as there are many parameters to be optimized (PTO coefficients, geometry, control algorithm, operating conditions

…), and these parameters are not independent. For example, the operating conditions set the sizing and geometry affecting the hydrodynamic performance, which affect the optimized PTO parameters or coefficients, and this causes a change in the control algorithm.

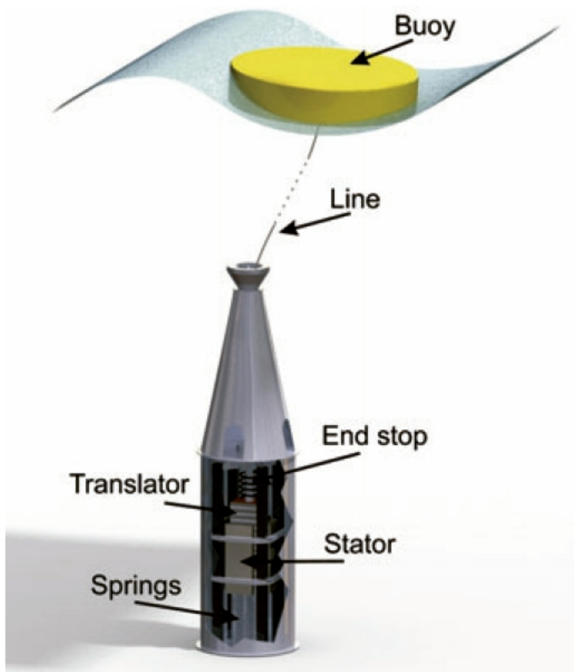

Figure 1: Point absorber coupled with a linear generator [3]

As mentioned earlier, WECs come in different types and operation modes, but the heaving point absorber offers many advantages over other types of WECs because of the low complexity and high reliability, which are important for an offshore platform as argued in [1], [2] and [4]. Also, coupling the heaving point absorber with a linear generator offers lower maintenance than that with other PTO techniques, and resonating the point absorber with the incoming waves offers relatively high efficiency as many control methods can be adopted.

There have been many attempts to optimize the heaving point absorbers, either by altering the geometry and operational coefficients, or by proposing new control methods to resonate the device with the incoming wave which maximizes the power output. A heaving point absorber was hydro-dynamically modeled to resonate with the incoming wave and was optimized with the change of the floater's radius as illustrated in [5]. An active phase control method for heaving point absorbers was proposed to optimize the power output [6]. The PTO damping and the natural resonating frequency of a heaving buoy were optimized for operating in the Australian seas [7]. Two shapes of buoys with different diameters and drafts were studied in an attempt to optimize a heaving point absorber [8]. It was concluded that the shape didn't have a considerable effect on the power output, while the increase of diameter results in an increase of power output for a 1 body WEC. The different geometric parameters that affect the resonance frequency, absorbed power and production cost were researched through a parametric study and optimization of a resonating heaving point absorber [9]. The power output of a heaving point absorber was optimized by applying a latching control method in a fully non-linear 3D CFD simulation of a floating spherical buoy [10]. It was concluded that the traditional boundary element methods overestimate the generated power. Non-dimensional hydrodynamic equations which are used to optimize the radius and draft of a cylindrical heaving point absorber were derived [11].

The heaving point absorber presents a simple and well optimized solution for harvesting wave energy with the main drawback being the operation at high ocean waves frequencies, as this will require very large masses and dimensions to lower the resonating frequency of the device. The solution to this is inclusion of a submerged oscillating body; the increase of the degrees of freedom lowers the resonating frequency and increases the captured power at low frequencies as illustrated in [3], [12], [13], and [14].

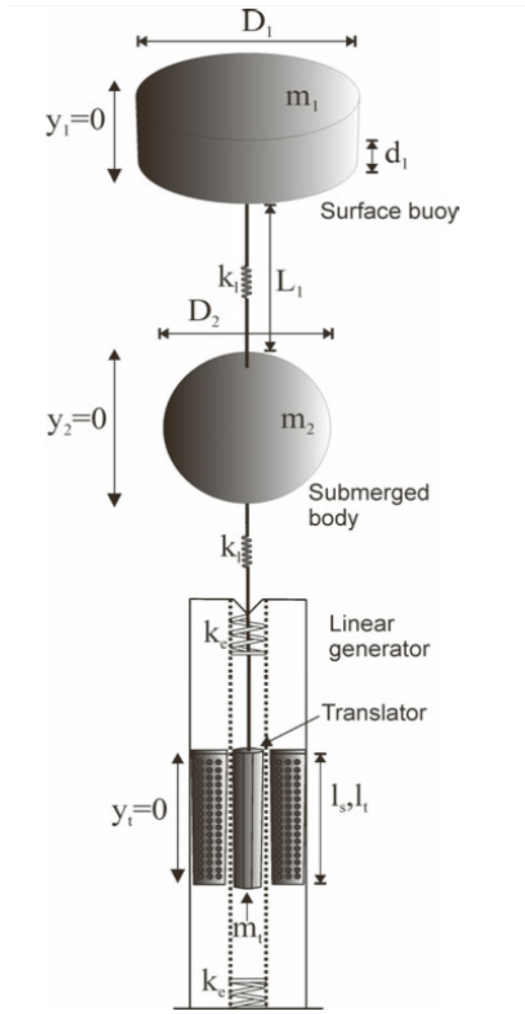

Figure 2: 2 body (heaving point absorber with a submerged body) WEC [15]

There have been many attempts to optimize two body WECs based on different disciplines: Bozzi et al [12] studied the power output of different dimensions of buoys with and without the inclusion of a submerged body in the Italian seas, and concluded that a smaller buoy with a submerged body can increase the capture width ratio by as much as 25% compared to a larger buoy without a submerged body. The effect of the dynamics of a two-body WEC with optimized PTO coefficients on the generated power was studied with the change of the submerged body mass [14]. A multiple degrees of freedom WEC was modeled, and the parameters affecting the power output were studied [16]. It was concluded that the added mass of the submerged body and the buoyancy of the floater have the greatest effect on the generated power. The response of a two-body WEC was studied under the variation of the design parameters with a focus on the hydrodynamic mathematical modeling [17]. It was concluded that the design parameters have a big impact on the generated power, especially those parameters related to the resonant frequency. A parametric study including geometric design parameters, PTO coefficients, and sea state for a two-body wave energy converter was conducted [18], and some dependencies between the altering parameters were concluded. A two body WEC using non-linear forces on the floater was optimized [19]. The performance was increased by using a curved shape of the buoy to decrease the viscous losses. The optimal operating conditions were established to maximize the power generation efficiency. A new optimization procedure for a two body WEC was suggested [20]. The new optimization procedure iterates all the design parameters (PTO damping, submerged added mass, buoy dimensions and draft) based on the various yearly operating conditions to conclude with an optimal design.

In spite of all the previous work done for optimizing the two body WECs, there is a lack of a comprehensive optimization study which incorporates all the different parameters affecting the output power, resonance frequency and bandwidth. Therefore, this paper will present a parametric study, design and optimization procedure which study the effects of the different parameters.

All these parameters could be intrinsically dependent, and the design and optimization procedure must be capable of studying the magnitude of each parameter's effect as well as the best combination of parameters that produces the highest power at a low operating frequency and with an acceptable bandwidth.

Taguchi method will be used to study and optimize a two body WEC based on 7 different parameters: PTO damping coefficient, PTO stiffness coefficient, diameter of the buoy, shape and volume of the submerged body, submerged body depth, and the buoy's draft. Taguchi method was simplified and widely applied for process optimization of chemical industries by Taguchi in the 1950's [21]. It can evaluate the response of a system with different parameters, and the magnitude of the effect of each parameter. Even though this method is developed and used in the industries, it is ideally applicable to optimize a two body WEC, considering the fact that all the different parameters are connected, and studying the effect of one or two design parameters won't have a great value for a comprehensive multidisciplinary wave energy harvesting system. After conducting the parameter study using Taguchi method, the parameter combinations of two optimal output targets are identified, one has the highest power and the other has the best resonance frequency and bandwidth. The parameter combinations would be iterated and optimized based on the Taguchi method outcomes to derive the final optimized system for the Australian ocean waves' state.

This paper is a part of a project dedicated to design a WEC for the Australian seas. According to [7] and [22] the biggest wave energy potential lies in the southern Australian coast with an average wave period between 8 s and 12 s. Thus, the low frequency operation is a main focus of the optimization procedure, and the inclusion of a submerged body is selected for the design.

The submerged body plays a role in increasing the captured power as well as reducing the resonant frequency due to the increase of the added mass and the system's inertia. The added mass is caused by the volume of water that the submerged body is trying to displace while oscillating. The shape of the submerged body would influence the added mass and the system inertia (like a cylinder for example) has a large effect on viscous damping coefficient. The increased viscous damping coefficient results in a decrease in the captured power [14] and [23]. Therefore, comparing the shapes of two different submerged bodies would present an interesting result for the parameter study.

The hydrodynamic coefficients will be simulated using the software Ansys Aqwa, the viscous damping coefficients will be estimated from literature, and the power will be calculated using a Matlab code in the frequency domain.

The rest of the paper is divided as follows: the mathematical dynamic model will be developed and described in the second section, the parameter study using Taguchi method will be presented in the third section, the results will be discussed in the fourth section, the design will be optimized and iterated in the fifth section, and the conclusions will be given in the last section.

2. Mathematical model

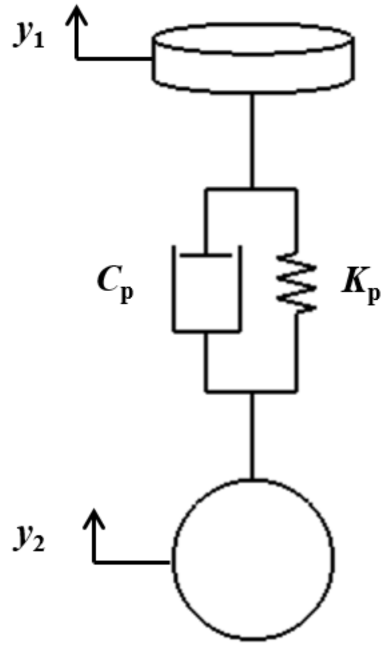

Figure 3: Sketch of the two body WEC system

Applying the Newton's second law to the two degrees of freedom system, in the frequency domain, where *j*=1 represents the floater, *j*=2 represents the submerged body, and y_j represents the displacement in the vertical heave direction, with $\dot{y}_j$ and $\ddot{y}_j$ representing the instantaneous velocity and acceleration of each of the floater and the submerged body respectively. Assuming potential flow theory which sets the wave as a regular sinusoid function (with the wave amplitude y_w taken in this work as 1m), the harmonic excitation can be assumed by: $y_j = Y_j e^{st}$, $s = i\omega$, where i is the imaginary unit, and ω is the wave frequency is rad/s. The PTO is placed between the buoy and the submerged body taking advantage of the relative movement between the two, and the hydrodynamic interactions between the floater and the submerged body are assumed to be negligible since the distance between them is 20 m or more [12].

For the floater:

$$M_1\ddot{y}_1 + k_p(y_1 - y_2) + c_p(\dot{y}_1 - \dot{y}_2) + k_h y_1 + F_{vd1} + c_{r1}\dot{y}_1 = F_{we1} \quad (1)$$

For the submerged body:

$$M_2\ddot{y}_2 + k_p(y_2 - y_1) + c_p(\dot{y}_2 - \dot{y}_1) + F_{vd2} + c_{r2}\dot{y}_2 = F_{we2} \quad (2)$$

F_{wej} is the wave excitation force exerted on the oscillating bodies composed of both the Froude-Krylov and the wave diffraction forces; according to the potential flow theory, this force is calculated by integrating the incident wave potential pressure (Froude-Krylov) and diffracted wave potential pressure (diffraction) over the surfaces of the oscillating bodies, this term can be solved using a BEM (Boundary Element Method) for the integral around the boundaries of the oscillating bodies leading to a linear wave excitation proportional to the wave elevation and can be written as: $F_{wej} = F_j e^{st}$, where F_j is the complex amplitude of the wave excitation force and is calculated using Ansys Aqwa.

M_j is the total mass of each of the floater and the submerged body, which is composed of both the physical dry mass m_j and the hydrodynamic added mass m_{aj}: $M_j = m_j + m_{aj}$, and c_{rj} is the radiation damping coefficient. The hydrodynamic added mass and radiation damping coefficient represent the radiation forces on the oscillating bodies, these parameters are also calculated using a BEM with Ansys Aqwa, and they represent the linear solution of the integral of the radiated wave potential over the surfaces of the oscillating bodies.

k_h is the hydrostatic stiffness of the floater, generating a spring stiffness effect due to the difference between the weight and the buoyancy forces. The submerged body has neutral buoyancy, resulting in the buoyancy force always equaling the weight force, and the absence of the hydrostatic spring force term in Equation (2).

The PTO force, F_p is simulated by a linear force of a spring damper system:

$$F_p = k_p(y_{j+1} - y_j) + c_p(\dot{y}_{j+1} - \dot{y}_j) \tag{3}$$

where k_p and c_p are the PTO's stiffness and damping coefficients respectively. This equation neglects the electrical circuit term of the linear generator which add another degree of freedom to the equations [24]. The effect of the electrical circuit term is included in the damping coefficient of c_p.

The viscous damping force is modeled according to the non-linear Morison equation:

$$F_{vd} = \frac{1}{2}\rho a_j c_{dj} \dot{y}_j^{\,2} \tag{4}$$

where ρ is the density of water, a_j is the cross sectional area of the body in question and c_{dj} is the dimensionless viscous damping coefficient. Since all other equations are linear and the viscous damping force equation is of the second order, it would be more convenient to linearize this equation based on the work done by [25] to solve all the equations in the frequency domain. The linearized viscous damping equation is:

$$F_{vd} = \frac{1}{2}\rho a_j c_{dj} \frac{8}{3\pi} V_{max} \dot{y}_j \tag{5}$$

where V_{max} is the maximum velocity reached by the oscillating body in the heave direction. The viscous drag damping forces on the floater are assumed to be negligible, especially compared to the wave excitation forces [26]. Therefore, c_{vd2} in Equation (3) is given by

$$c_{vd2} = \frac{1}{2}\rho a_2 c_{d2} \frac{8}{3\pi} V_{max} \tag{6}$$

By applying Fourier transform onto Equations (1) and (2), and neglecting the radiation damping on the submerged body [14] (this will also be shown the next section where the hydrodynamic simulations are presented), the displacements of the floater and submerged oscillating bodies are given by the following equation:

$$\begin{Bmatrix} \frac{Y_1}{y_w} \\ \frac{Y_2}{y_w} \end{Bmatrix} = \begin{bmatrix} M_1 s^2 + (c_\mathrm{p} + c_{\mathrm{r}1})s + (k_\mathrm{p} + k_\mathrm{h}) & -c_\mathrm{p} s - k_\mathrm{p} \\ -c_\mathrm{p} s - k_\mathrm{p} & M_2 s^2 + (c_\mathrm{p} + c_{\mathrm{vd}2})s + k_\mathrm{p} \end{bmatrix}^{-1} \begin{Bmatrix} \frac{F_1}{y_w} \\ \frac{F_2}{y_w} \end{Bmatrix} \quad (7)$$

The PTO is connected between the float and the submerged body, the average power is calculated as follows:

$$P_{average} = \frac{1}{T}\int_0^T c_p(\dot{y}_1 - \dot{y}_2)^2 dt = \frac{1}{2}\omega^2 c_p |Y_1 - Y_2|^2 \quad (8),$$

where T is the period of the wave in s. Y_1-Y_2 can be calculated from solving equation (7).

3. Parametric study

As discussed earlier, Taguchi method is a parameter study and optimization method simplified and applied by Taguchi in the 1950s for optimization of industrial chemical processes. This method studies the response of a system output for variation of different parameters, which are generally correlated in a way or the other. It is based on statistical analysis which studies the sensitivity of the target variables to the input variables in order to improve the quality of the product/outcome/design. Taguchi method is best suitable for the systems where their optimum operational conditions are dependent on different input parameters correlated with each other. The effect of each parameter on the system in Taguchi method is similar to a signal/noise ratio. Taguchi method should be applied in the second and third phases of product design. For WECs, the first phase of design would be to establish a concept, for the case of this paper, a two-body point absorber which utilizes the relative movement of a buoy and submerged body imposed by the wave loadings to harvest wave energy. The second stage is referred as robust design, and it is to determine all the different parameters and dimensions of the design, these are the parameters in Table 1. The third stage is to optimize the design with a parametric study of the different input parameters affecting the output performance of the WEC using Taguchi method. This method relays on orthogonal arrays which significantly reduces the number of iterations and simulations needed to determine the effect of each parameter on the desired output performance [27]. Therefore, Taguchi method's mathematical formulations and orthogonal arrays formulate the L8 matrix presented in Appendix A which can study the effect of 7 different dependent variables on the performance of the proposed two-body WEC without the need to find the mathematical correlations between them. The parametric study and simulations are conducted using both Microsoft Excel and Matlab software, with the hydrodynamic parameter inputs from Ansys

Aqwa simulations. This section will present the parametric study of Taguchi method. Optimizations based on this method will be presented later on.

This paper would study the effect of seven different parameters on the output performance of a two body WEC. The output performance is represented by the maximum average power generated by the system, the resonant frequency and the operational bandwidth. The parameters chosen are preferably set as two extreme levels.

Table 1: Taguchi method parameters

		Level 1	Level 2
Parameter 1	PTO damping	Off-control	On-control
Parameter 2	PTO stiffness	min	max
Parameter 3	Diameter of buoy	min	max
Parameter 4	Submerged body	cylinder	sphere
Parameter 5	Submerged body Volume	min	max
Parameter 6	Buoy's Draft	min	max
Parameter 7	Submerged body depth	min	max

Table 1 presents the different parameters studied by Taguchi method. Parameter 1, the PTO damping, off-control would be set as Level 1 which has a constant damping coefficient value equal to 100 $kNsm^{-1}$. The on-control would be set as Level 2. The on-control algorithm is the impedance matching control scheme where the PTO damping coefficient is changing with the ocean wave excitation frequency and have to match the variable external hydrodynamic and viscous damping of the system, that is, $c_p = c_{r1} + \frac{1}{2}\rho a_2 c_{d2} \frac{8}{3\pi} V_{max}$. A submerged body is added to the system, which is considered as a passive control method [3]. Therefore, the PTO damping is adjusted and changed to be equal to the external damping, which should refine the performance further. Parameter 2, the PTO stiffness, would be set in two levels; 100 kN/m in Level 1 and 200 kN/m in Level 2. Parameter 3, the Buoy's diameter, will be set in two levels, 4 m in Level 1 and 6 m in Level 2. It is known that increasing the size of the buoy would increase the absorbed power. Parameter 4, the shape of the submerged body is set to be a cylinder in Level 1, and to be a sphere in Level 2. Having a sphere as a submerged body should increase the power because of the low viscous damping of the system, but having a cylinder as a submerged oscillating body should have a lower power due to the large viscous damping of the system, a lower resonant frequency and a larger bandwidth because of the large added mass, viscous damping and system inertia. Parameter 5, the volume of the submerged body, is set as 33.51 m^3 in Level 1 and 113.1 m^3 in Level 2 (diameter being altered between 4 m and 6 m) with the same cross sectional area of the sphere and the cylinder in order to consistently compare their viscous damping coefficient, the hydrodynamic coefficients, the physical weights, and volumes. Parameter 6, the buoy's draft, is set in two levels, 1 m in Level 1 and 2 m in Level 2. Increasing the draft should decrease the radiating capabilities of the buoy, and therefore lowers the extracted power. Finally, Parameter 7, the depth of the submerged body, is set in two levels; 20 m for Level 1, and 40 m for Level 2. Both these depth values should prevent the submerged body from the disturbance in the radiating capabilities caused by the hydrodynamic effects between the floating and submerged bodies. The hydrodynamic effect should be limited to the excitation force on the submerged body. Appendix A includes the full Taguchi L8 matrix

Table 2: Taguchi method L8 matrix

	Parameter 1	Parameter 2	Parameter 3	Parameter 4	Parameter 5	Parameter 6	Parameter 7
System	PTO damping (N.s/m)	PTO Stifness (N/m)	Diameter of buoy (m)	Submerged body geometry	Submerged body Volume (m^3)	Buoy's Draft (m)	Submerged body depth (m)
1	cp=100000	k1=100,000	4	Cylinder	33.51	1	20
2	cp=100000	k1=100,000	4	Sphere	113.1	2	40
3	cp=100000	k2=200,000	6	Cylinder	33.51	2	40
4	cp=100000	k2=200,000	6	Sphere	113.1	1	20
5	Variable	k1=100,000	6	Cylinder	113.1	1	40
6	Variable	k1=100,000	6	Sphere	33.51	2	20
7	Variable	k2=200,000	4	Cylinder	113.1	2	20
8	Variable	k2=200,000	4	Sphere	33.51	1	40

Table 2 presents the Taguchi method L8 matrix; the columns present every parameter and their levels, while every row combines different parameters and their levels to represent a standalone system. S.b. stands for submerged body. It should be noted that the fourth parameter not only affects the hydrodynamic properties of the system (wave excitation force, added mass and radiation damping), but also has a considerable impact on the system's dynamics and generated power through the difference in the viscous damping coefficient which is chosen to be 0.1 for the sphere and 1 for the cylinder, these viscous damping coefficient values are derived from the literature for smooth bodies operating at the high Reynolds number [23, 28-31].

The Taguchi method matrix contains 8 different test runs or systems, each with different set of parameters. Every system is modeled using a CAD model and simulated in Ansys Aqwa to calculate its hydrodynamic coefficients. For example, System 4 is modeled using a CAD model and simulated in Ansys Aqwa as shown in Figure 4. These coefficients are used for calculation of the power vs frequency curve of each system from Equation (7) and (8) using Matlab codes.

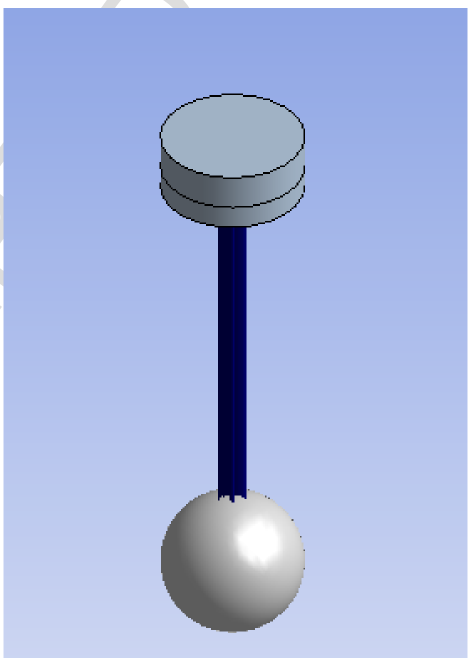

Figure 4: System 4 modeled in Ansys Aqwa

Figures 5-10 represent the results simulated in Ansys Aqwa. Figures 5, 6 and 7 represent the buoy's excitation force, added mass and radiation damping coefficient respectively for the eight systems, while Figures 8, 9 and 10 represent the submerged body's excitation force, added mass and radiation damping respectively for the eight systems.

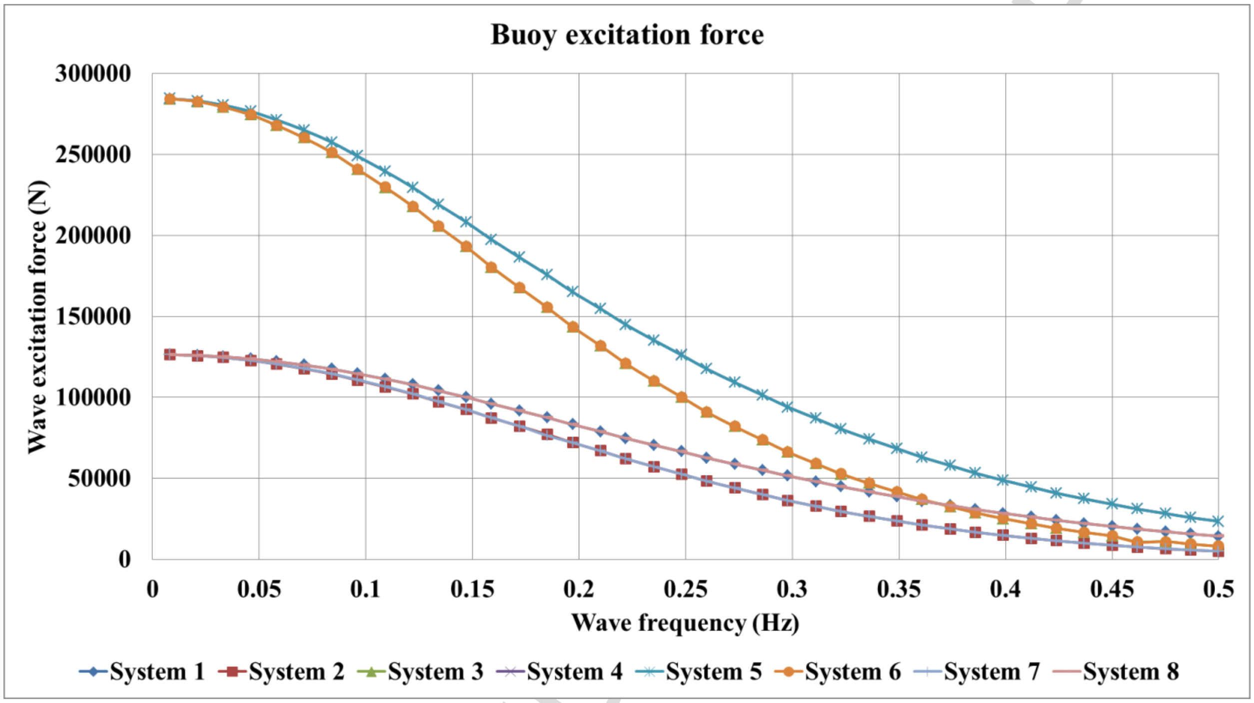

Figure 5: Buoy's excitation force for the 8 systems

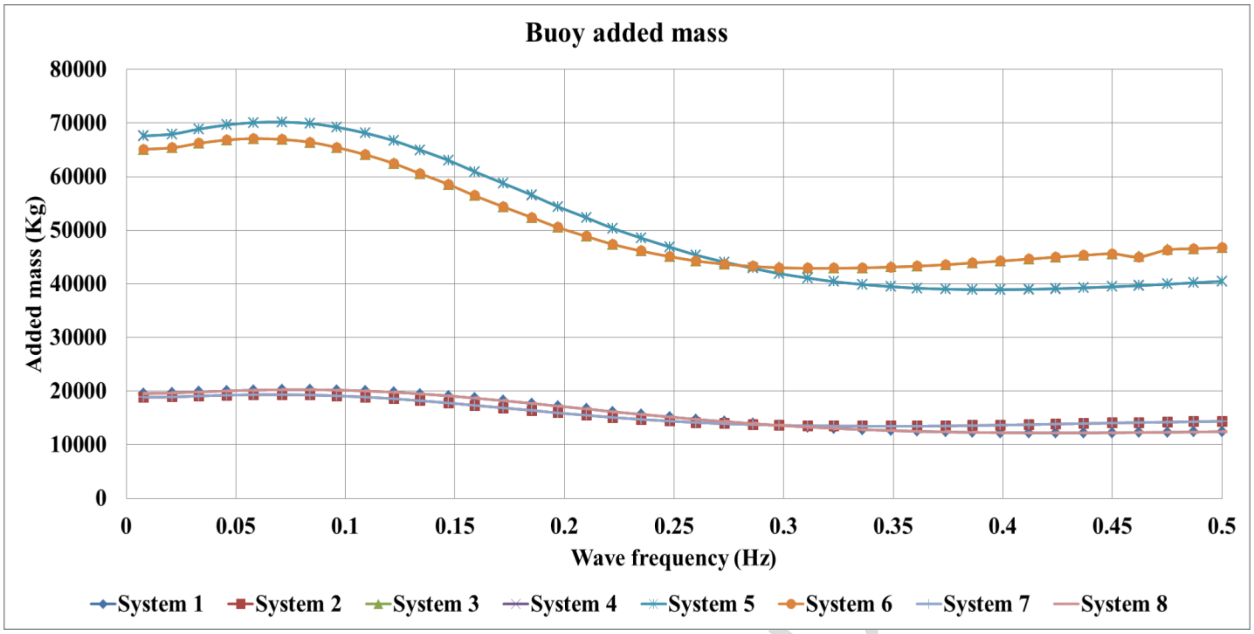

Figure 6: Buoy's added mass for the 8 systems

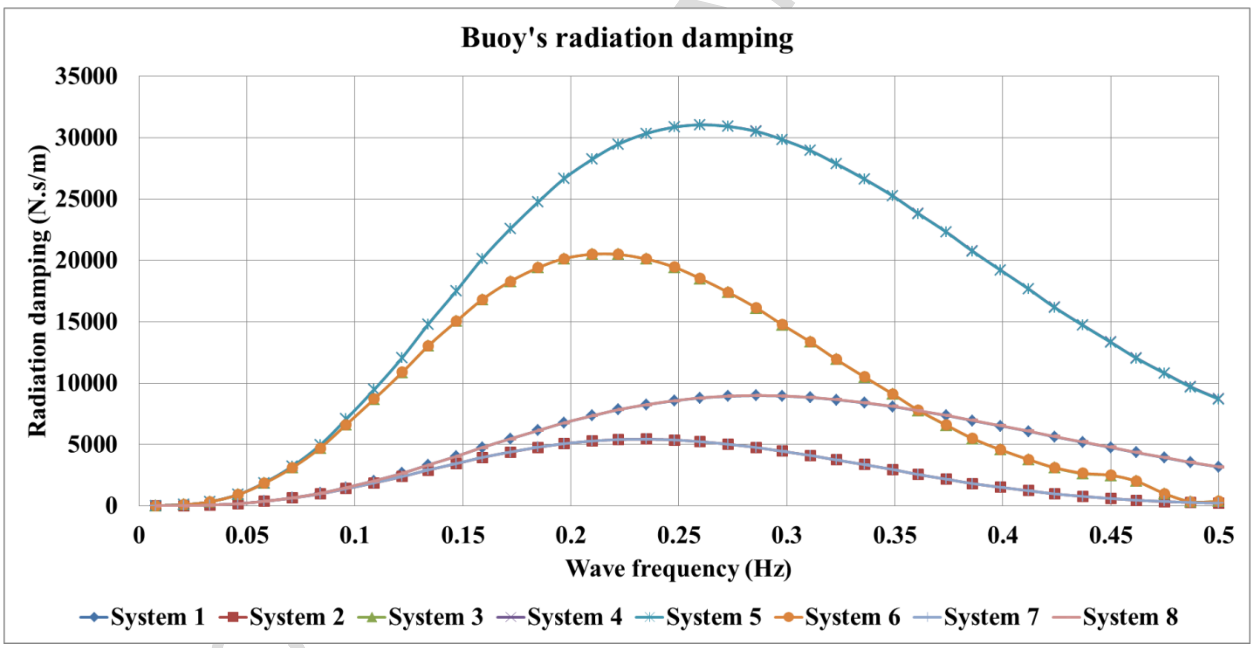

Figure 7: Buoy's radiation damping for the 8 systems

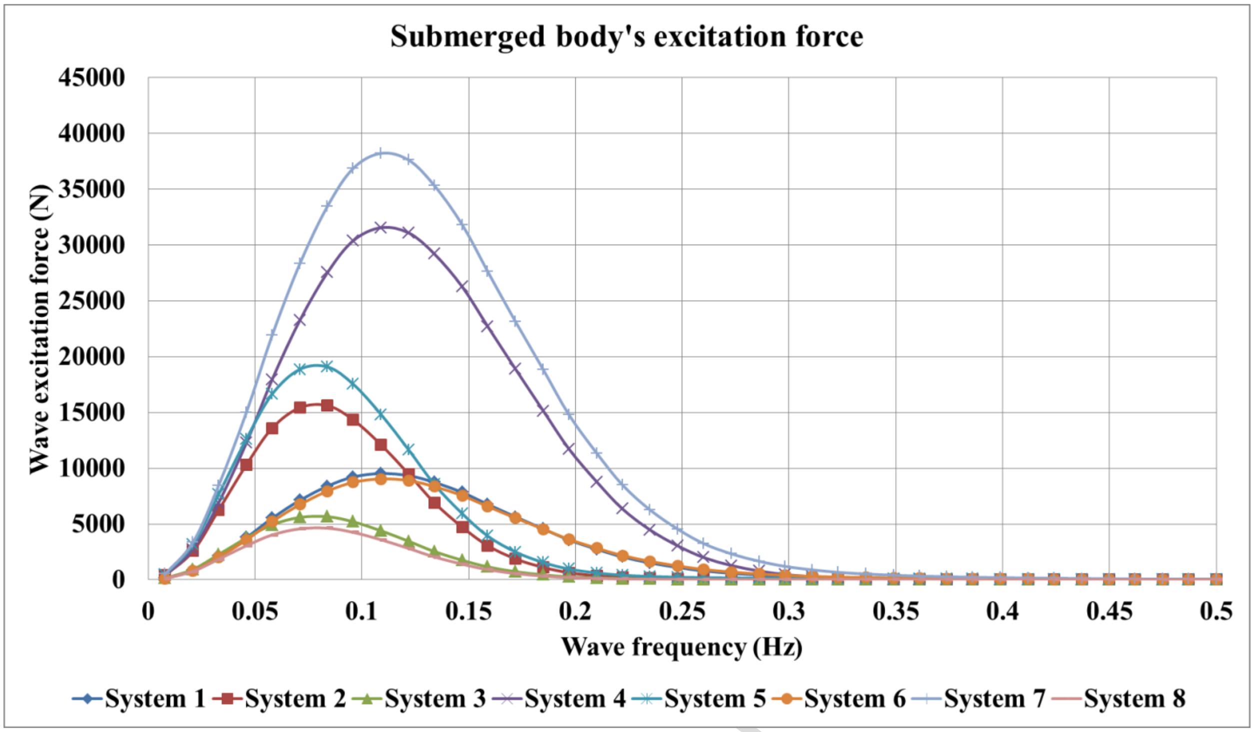

Figure 8: Submerged body's excitation force for the 8 systems

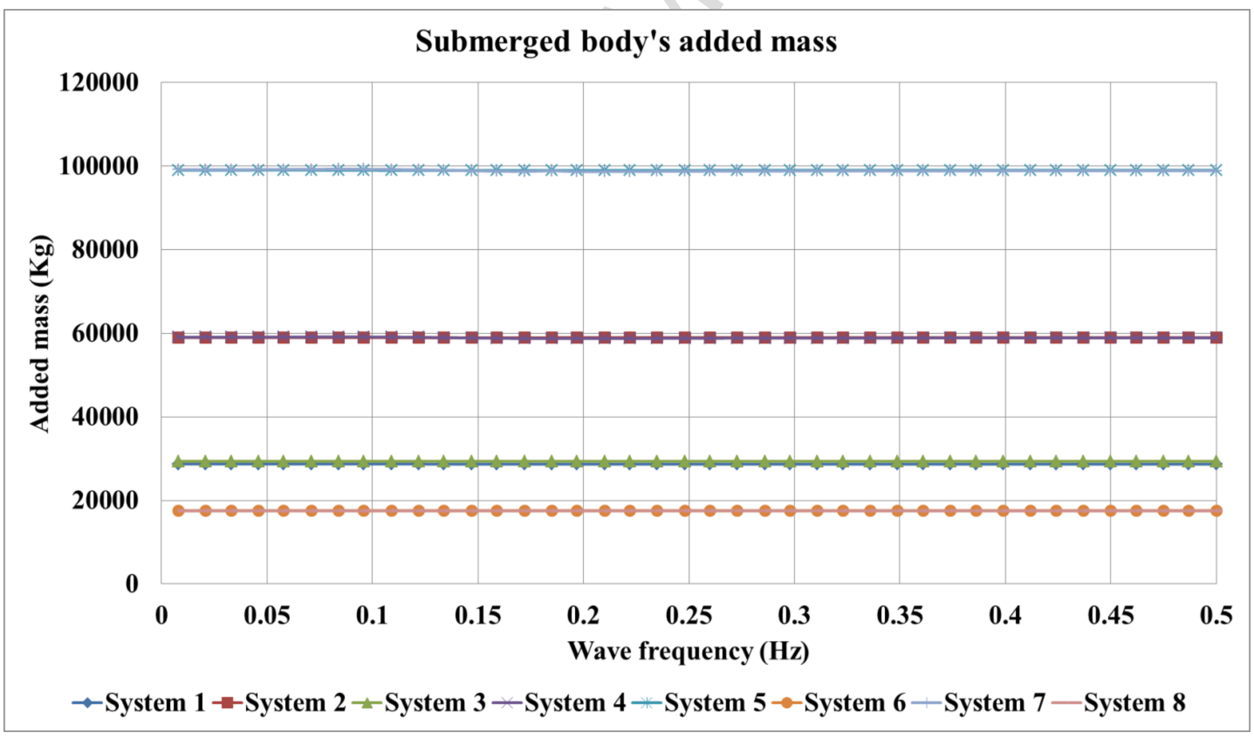

Figure 9: Submerged body's added mass for the 8 systems

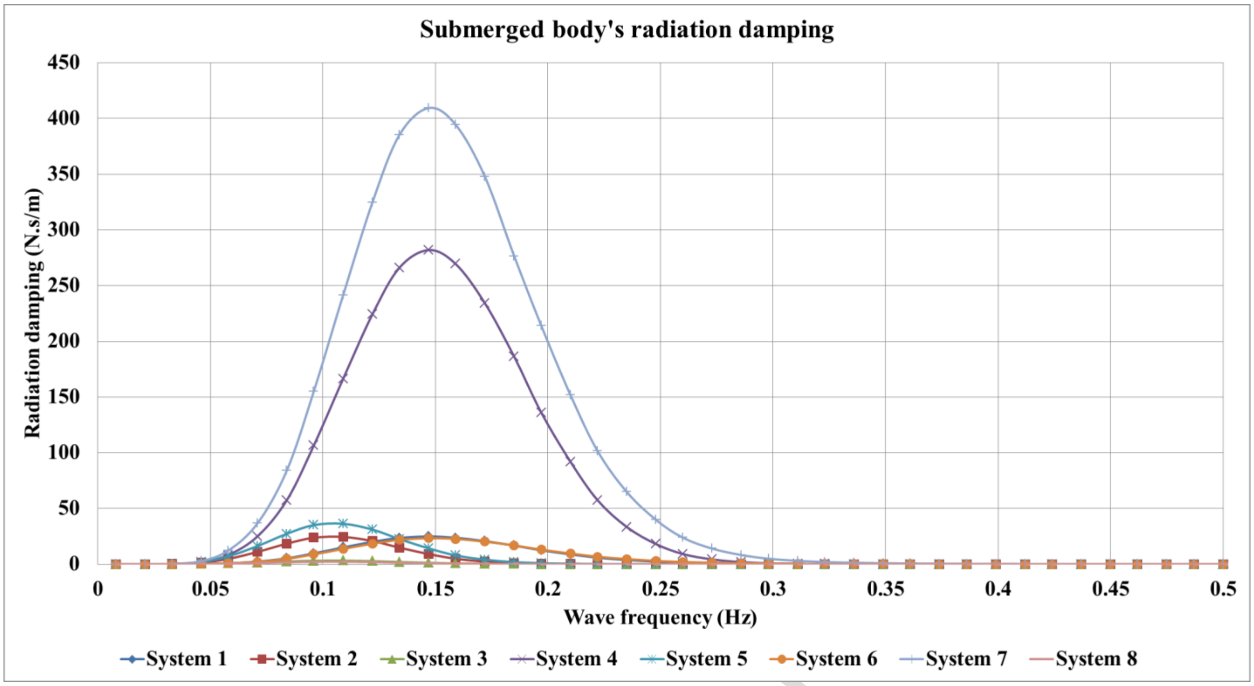

Figure 10: Submerged body's radiation damping for the 8 systems

The first apparent conclusion from the Ansys Aqwa results is that the radiation damping of the submerged body is negligible compared to the radiation damping of the buoy as shown in Figures 5 and 10. Also, the depth effect is only reflected by a peak frequency difference and magnitude difference of the excitation force exerted on the submerged body; this can be seen in Figure 8. Systems 5 and 7 for example have the same shape and volume of the submerged body, but System 7's submerged body is placed at a smaller depth than System 5, hence System 7's submerged body has a 1900N larger wave excitation force than System 5's submerged body, the same observation can be made between Systems 2 and 4, 1 and 3, and Systems 6 and 8. The rest of the systems with the same depth have the same hydrodynamic coefficients, which confirm the assumption that the submerged body is placed at a depth where there are no hydrodynamic interactions between the two oscillating bodies. Taking a closer look at each of the above figures; Figure 5 reflects that the buoy's wave excitation force increases with the buoy's diameter. As

Systems 3, 4, 5 and 6 have a larger buoy diameter than the other systems (6 m vs. 4 m) and thus having a larger wave excitation force in Figure 5. Also, the draft increase causes a decrease in the wave excitation force. As for example Systems 3, 4, 5, and 6 all has the same buoy diameter, but Systems 3 and 6 both have a larger draft of 2 m than Systems 4 and 5, and thus they have a lower wave excitation force as seen in Figure 5. The same comparison can be made between Systems 1, 4 and Systems 3, 7. Systems 3 and 4 have a larger buoy diameter, a wider wave pressure surface area than Systems 1 and 7 (6 m vs. 4 m), which results in higher hydrodynamic performance all around of Systems 3 and 4 than that of Systems 1 and 7. This is because the shape and the volume have the largest effect on the wave excitation force, added mass and radiation damping. The decreased wave excitation force of System 3 and 6 is due to the decrease in the radiating capabilities out of the increased draft. This is because the extra submerged depth of the buoy decreases its interaction with the incoming wave, and therefore decreases the wave excitation force on the buoy. This is also manifested in Figure 7 where the extra draft highly reduces the radiation damping of the buoy. This is because Systems 3, 4, 5, and 6 all have the same buoy diameter, but Systems 3 and 6 both have a larger draft of 2 m, and thus they have lower radiation damping as seen in Figure 7. The same comparison can be made between Systems 1, 4 and Systems 3, 7. In Figure 6, it is noticed that the diameter also has the largest effect on the added mass, and the draft has a slight effect. This is because Systems 3, 4, 5 and 6 have a larger buoy diameter than the other systems (6 m vs. 4 m) and thus having more added mass (2 to 3 times higher).

Figure 8 represents the wave excitation force exerted on the submerged body, it is expected to see that the wave excitation force increases with the increase in the submerged body's size. It is also noticed that the wave excitation force exerted on the cylinder is higher than the one exerted on a sphere for the same volume and depth. As for example Systems 4 and 7 both have the same submerged body volume (113.1 m^3) and the same depth (20 m), but it is seen from Figure 8 that the excitation force exerted on System 7's cylindrical submerged body is higher than the one exerted on System 4's spherical submerged body. The same comparison can be made between Systems 5 and 2. The difference is less pronounced in other systems because of the low excitation force. Also, the increase in the submerged body's depth decreases the wave excitation force, which is expected, since the extra depth of the submerged body further away from the surface of the water limits the interaction of the submerged body with the surface wave. Figure 9 represents the added mass of the submerged body of each of the 8 systems. It is noticed that the added masses are constant versus wave frequency. Similar to the outcome trend of Figure 8, the added mass of a cylinder is higher than that of the sphere for the same volume. As for example Systems 5 and 7 have the cylindrical submerged body of a volume of 113.1 m^3 and possess a higher added mass of 100,000 Kg than Systems 4 and 2 which have 60,000 Kg of added mass at the same volume but with a spherical submerged body. Finally, Figure 10 shows the cylindrical submerged body having higher radiation damping. The increase in depth would reduce the dynamic interactions between the surface wave and the submerged body, thus reducing the radiation damping, this follows the same trend as the outcomes of Figure 8.

The main noticeable behavior of Figures 8-10 is that the cylindrical shape of the submerged body exhibits higher hydrodynamic properties than the spherical shape, and this is due to the cylindrical flat shape displacing more volume of water while oscillating, thus increasing the system's inertia and enhancing the hydrodynamic properties while operating underwater.

These results are imported to a Matlab code which is based on Equation (8) to calculate the power (W) vs. frequency (Hz) curve shown in Figure 11 and the output of each system in the Taguchi method's matrix.

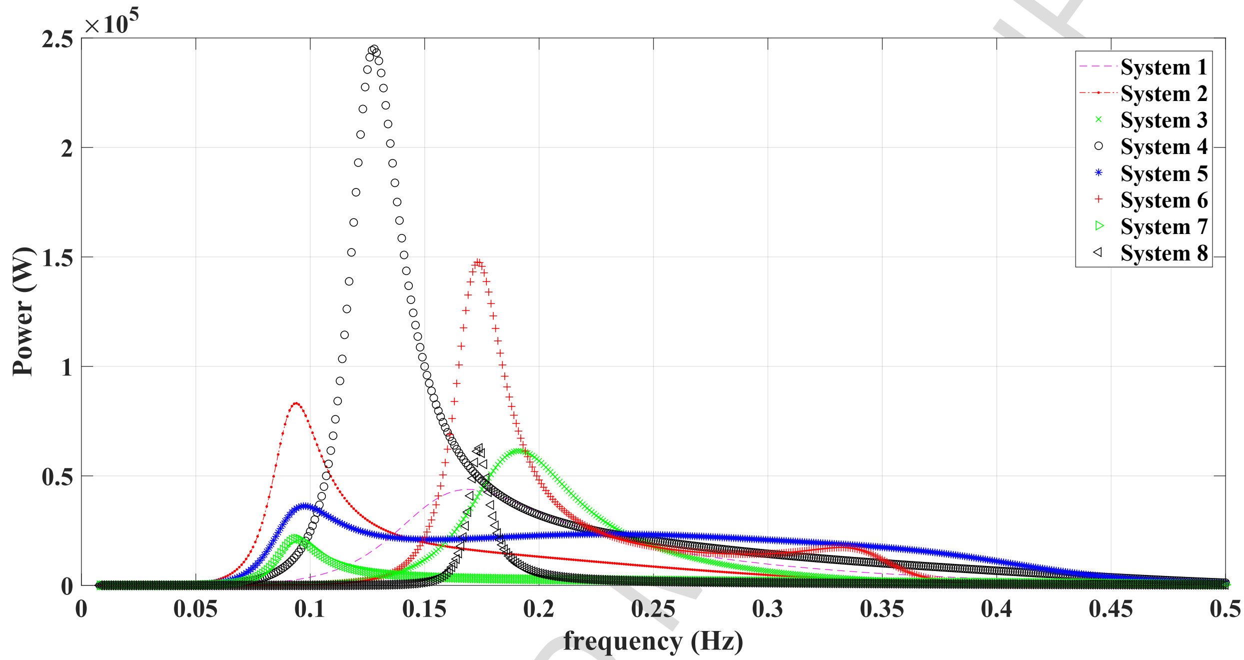

Figure 11: Output power vs frequency for the 8 systems

4. Discussions

Figure 11 shows the ouput power vs. frequency for the 8 systems, and Table 3 includes numerical values of the results in Figure 11. The three main output performance attributes presented are the maximum power, the resonant frequency, and the bandwidth. It should be noted that the resonant frequency is desired to be low for two reasons: a) it is extremely hard to lower the resonant frequency of a designed system, while it is easy to increase it; b) this paper is a part of a project dedicated to design a wave energy converter for the Australian oceans where the operating frequency is relatively low (0.0833Hz-0.125Hz). In the wave energy conversion systems, the bandwidth is usually measured as the frequency range where the generated power is 50% of the maximum power, also known as the half power bandwidth.

Table 3: Output performance attributes of the 8 systems

System	Max Power (kW)	Resonance frequency (Hz)	Bandwidth (Hz)
1	43.806	0.170	0.087
2	83.152	0.095	0.032
3	61.432	0.192	0.059
4	245.000	0.129	0.030
5	36.210	0.098	0.258
6	147.620	0.174	0.028
7	21.327	0.095	0.016
8	62.690	0.175	0.011

It is seen from Table 3 that System 4 resulted in the highest produced power of 245 kW, which is expected considering it has a large buoy, a large submerged body and low viscous damping (sphere). Systems 2 and 7 demonstrated the lowest resonant frequency at 0.095 Hz, followed by System 5 of 0.098 Hz, the undamped resonant frequency is $f_r = \sqrt{\frac{k_h + k_p}{\Sigma_{j=1}^{j=2} M_j}}$, and the results are expected since the systems with the large submerged bodies had the lowest resonant frequency because of the large physical and added mass produced by the large volumes. System

5 had the largest bandwidth with 0.258 Hz of operational range. Since System 5 has the largest resonant damping and a resonant frequency very close to the resonant frequency of Systems 2 and 7 which is the minimum resonant frequency of all the eight systems, equal to 0.095 Hz. System 5 will be qualified as the best in terms of operating frequencies, and System 4 will be qualified as the best in terms of maximum generated power. The large bandwidth and resonant damping of System 5 are correlated with the high system inertia and viscous damping introduced by the large cylindrical oscillating submerged body.

The systems of the best performance presented predictable results, but the Taguchi method outcomes do not only present the best combination in favor of a specific output performance attribute, but also it can study the magnitude of the effect each parameter has on the performance.

Table 4: Parameter effects on the maximum output power

		Level 1 Power (kW)	Level 2 Power (kW)	Power Effect (kW)	Power Effect (%)
Parameter 1	PTO damping	108.348	66.962	-41.386	44.064
Parameter 2	PTO Stifness	77.697	97.612	19.915	21.204
Parameter 3	Diameter of buoy	52.744	122.566	69.822	74.340
Parameter 4	Submerged body	40.694	134.616	93.922	100.000
Parameter 5	Submerged body Volume	78.887	96.422	17.535	18.670
Parameter 6	Buoy's Draft	96.927	78.383	-18.544	19.744
Parameter 7	Submerged body depth	114.438	60.871	-53.567	57.034

Table 4 shows the numerical magnitude of the effect of each parameter on the maximum generated average power. The third column is the average of the maximum power for all the systems set with level 1, while the fourth column is the average of the maximum power for all the systems set with level 2, the fifth column is the difference between the third and the fourth, and finally, the last column is the percentage effect value of the fifth column with respect to the maximum power. All the parameter effect tables in this paper will have the same structure.

Parameter 4, the shape of the submerged body, had the biggest effect on the maximum generated power with a 93.922 kW increase in average power going from a cylindrical submerged body to a spherical submerged body. That is because the added viscous damping of a cylinder is much larger than the viscous damping of a sphere. The buoy's diameter had the second biggest effect on maximum generated average power, as increasing the diameter from 4m to 6m resulted in a 69.822 kW increase in the maximum output power. This is nothing surprising as it is widely known that for heaving point absorbers increasing the volume of the floater will increase the absorbed power. One rather unexpected result is the magnitude of the effect the depth of the submerged body on the maximum generated power. Increasing the depth of the submerged body from 20m to 40m resulted in a 53.567 kW decrease in the maximum generated power, which is almost 77% of the magnitude of the buoy's diameter effect. The physical cause is due to the three to four times reduction and peak frequency shift of the wave excitation force on the submerged body. Since the submerged body's physical and added masses are much larger than the buoy's, the changes of the wave excitation force on the submerged body have a higher manifestation in the system's dynamics. The PTO damping coefficient had an unusual effect on the power, as applying the control scheme, where the PTO damping coefficient is changing and equal to the external mechanical damping, should increase the maximum generated power. However, in this case the power was reduced by 41.386 kW. This indicates that the constant PTO damping coefficient value chosen in parameter 1, level 1 is close to the optimal value where the maximum power is harvested [14, 32], and that impedance matching for two-body point absorbers are not as effective as that for one-body point absorbers. This might be due to non-linear viscous damping forces acting on the submerged body. It should be noted that other control algorithms such as latching or phase control might give different results, but these control algorithms might have dominating effects on the performance of the proposed two-body point absorber as they have been shown being able to increase the captured power by a factor of two

[33]. Therefore, a simple impedance matching scheme was chosen for this study in order to properly evaluate the effects of the other geometric and hydrodynamic design parameters. The PTO stiffness, submerged body volume and buoy's draft had minor effects on the maximum generated power ranging between 17 kW and 20 kW, as their effects on the resonant frequency and the bandwidth are more manifested. However, it should be noted that increasing the draft reduces the maximum power. This is caused by the reduction in the radiating capabilities (reduction in the wave excitation force and the radiation damping).

Table 5: Parameter effects on the resonant frequency

		Level 1 resonance frequency (Hz)	Level 2 resonance frequency (Hz)	Frequency Effect (Hz)	Frequency Effect (%)
Parameter 1	PTO damping	0.147	0.136	-0.011	14.97
Parameter 2	PTO Stifness	0.134	0.148	0.014	18.37
Parameter 3	Diameter of buoy	0.134	0.148	0.015	19.73
Parameter 4	Submerged body	0.139	0.143	0.005	6.12
Parameter 5	Submerged body Volume	0.178	0.104	-0.074	100.00
Parameter 6	Buoy's Draft	0.143	0.139	-0.004	5.44
Parameter 7	Submerged body depth	0.142	0.140	-0.002	2.72

Table 5 presents the numerical values of the magnitude of the effect each parameter has on the resonant frequency using the same method as Table 4. There is one notable parameter which had a great effect on the resonant frequency and that is the submerged body volume. Increasing the volume of the submerged body from 33.51 m^3 to 113.1 m^3 (the diameter from 4 m to 6 m) will decrease the resonant frequency by a 0.074 Hz. This is due to the increase of physical mass and added mass with the increase of the volume, which reduces the resonant frequency according to the equation $f_r = \sqrt{\frac{k_h + k_p}{\sum_{j=1}^{j=2} M_j}}$. The rest of the parameters had a lower effect on the resonant frequency. The PTO stiffness increase will increase the resonant frequency as the stiffness increases the value of the numerator in the previous equation. The diameter of the buoy increase will increase both the hydrodynamic stiffness k_h and added mass and will therefore increases the values of both the denominator and numerator in the undamped resonant frequency equation, and will cause a slight increase of the resonant frequency by 0.015 Hz as a result. The rest of the parameters had a negligible effect on the resonant frequency.

Table 6: Parameter effects on the bandwidth

		Level 1 Bandwidth (Hz)	Level 2 Bandwidth (Hz)	Bandwidth effect (Hz)	Bandwidth effect (%)
Parameter 1	PTO damping	0.052	0.079	0.027	33.563
Parameter 2	PTO Stifness	0.101	0.029	-0.072	90.125
Parameter 3	Diameter of buoy	0.037	0.094	0.057	71.688
Parameter 4	Submerged body	0.105	0.025	-0.080	100.000
Parameter 5	Submerged body Volume	0.046	0.084	0.038	46.938
Parameter 6	Buoy's Draft	0.097	0.034	-0.063	78.375
Parameter 7	Submerged body depth	0.040	0.090	0.050	62.313

Table 6 presents the numerical value of the magnitude of the effect each parameter has on the bandwidth using the same method as Table 4. The shape of the submerged body had the largest effect on the bandwidth with a bandwidth decrease of 0.08 Hz going from a cylinder to a sphere. This is due to the increase of the system's inertia caused by the cylindrical shape and the increase of both the viscous and radiation damping. The submerged body depth, the buoy's draft, submerged body volume and diameter of the buoys all had a similar effect on the bandwidth because of the change in the hydrodynamic properties of the system. Increasing the buoy's draft reduced the bandwidth because of the decrease in the radiating capabilities. Increasing the volume of the submerged body increases the bandwidth because of the increase of the viscous damping. Finally, increasing the diameter of the buoy increases the bandwidth because of the increase in the hydrodynamic properties. The PTO damping had a negligible effect on the bandwidth because the difference between the variable damping and the constant damping is small. The PTO damping would have larger effect on the bandwidth if the difference between the variable damping and the constant damping is large. Finally, the PTO stiffness had a very interesting effect on the bandwidth. This parameter wasn't expected to have an effect on the system's bandwidth, as it is widely known that in resonant oscillating systems, the system's stiffness affects the resonant frequency while the damping affects the bandwidth. Doubling the PTO stiffness reduced the bandwidth by 0.072 Hz, therefore, the PTO stiffness is the second largest parameter affecting bandwidth after the submerged body's shape. From Figure 7 and the viscous damping equation of the submerged body; it is seen that both the radiation and viscous damping values (the maximum viscous damping force would occur at the region of maximum submerged body velocity) change with the frequency. The higher PTO stiffness value would increase the resonant frequency of the system moving the resonant power peak further away from the area with the largest viscous and radiation damping, thus reducing the system's bandwidth.

5. Optimization

Section 4 presented a parametric study of a two body WEC, and the effect of each parameter on the maximum generated power, resonant frequency and bandwidth has been investigated.

This section will present an optimization method based on the Taguchi method's outcomes in an attempt to design a two- body WEC suitable for the Australian oceans where the ocean wave's frequencies change between 0.0833 Hz and 0.125 Hz. System 4 produced the highest average power of 254 kW but with a high resonant frequency at 0.129 Hz and a relatively small bandwidth at 0.0296 Hz. On the other hand, System 5 presented the best performance in terms of operational frequency with a low resonant frequency of 0.098 Hz and a large bandwidth of 0.258 Hz, but a very low maximum power of 36.21 kW. Having large power but a high operational frequency isn't practical, and having a low operational frequency with low power output isn't efficient. Therefore, based on the outcomes of the fourth section, Systems 4 and 5 will undergo an optimization procedure in order to increase the output power of System 5, and reduce the resonant frequency and increase the bandwidth of System 4. In System 5, increasing the power output will have a negative effect on the resonant frequency and bandwidth, while in System 4, this optimization of the operation frequency and bandwidth will have a negative effect on the power output, but the goal is to iterate and compromise in order to design a system with acceptable power output and can operate in the Australian oceans with a relatively large bandwidth.

The optimizations done on System 4 without changing its fundamental shape are:

- Reducing the PTO stiffness from 200 kN/m to 100 kN/m.
- Decreasing the buoy’s draft from 1 m to 0.7 m.
- Increasing the depth of the submerged body from 20 m to 40 m.
- Increasing diameter of the submerged body from 6 m to 7 m.

The first change targets reduction of the resonant frequency, the last three changes target broadening the bandwidth and should increase the operational range of the system, while the last change targets the increase of both the physical and added masses of the submerged body which also helps to reduce the resonant frequency.

The optimizations done on System 5 without changing its fundamental shape are:

- Increasing the diameter of the buoy from 6 m to 7 m.
- Decreasing the depth of the submerged body from 40m to 20m.

Both these optimizations should increase the captured power with a considerable increase of the system’s hydrodynamic performance.

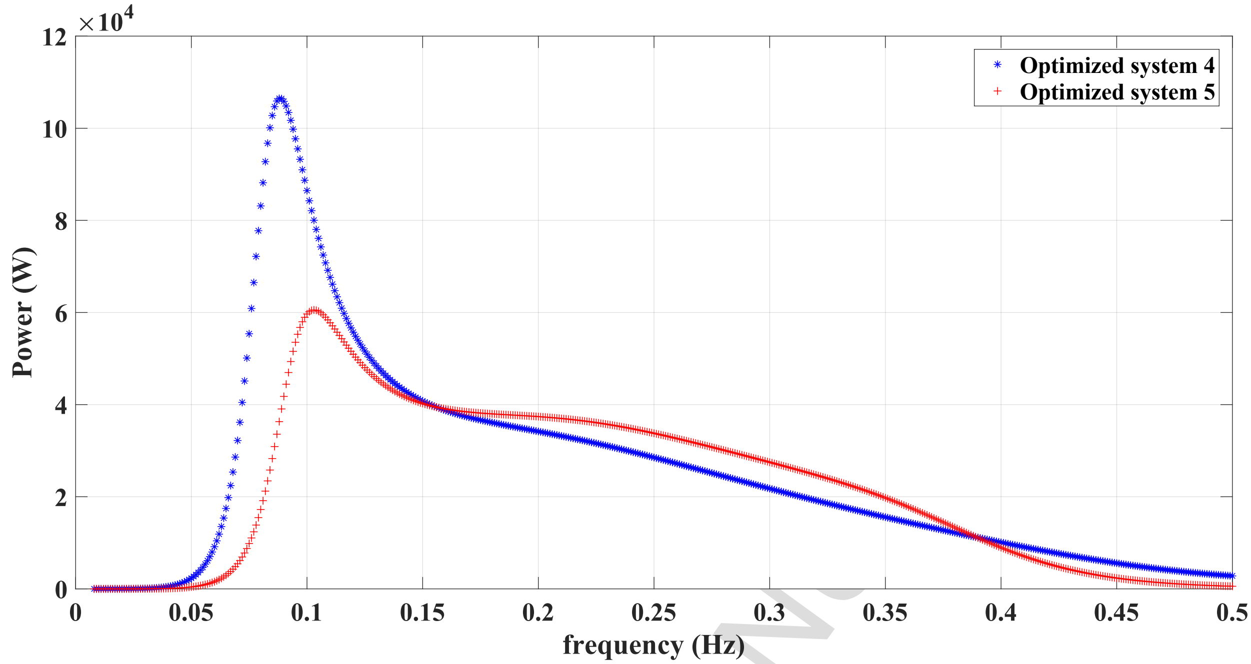

Figure 12: Optimized systems' output power vs. frequency

Table 7: Performance of the optimized systems

System	Max power (kW)	Resonance Fr (Hz)	Bandwidth (Hz)	Bandwidth @50% max power (Hz)
4 optimized	106.470	0.089	0.048	0.048
5 optimized	60.548	0.104	0.193	0.193

Figure 12 represents the power vs. frequency curve, and Table 7 represents the numerical values for the output performance of both `the optimized systems. System 4's maximum captured power has decreased because of the decrease in the hydrodynamic capabilities of the system caused by the increase in the submerged body's depth and the increase of the viscous damping with the increase of the submerged body's volume, but the resonant frequency and bandwidth are much more appropriate because of the optimizations applied. As for System 5, the maximum captured power has almost doubled but at the price of a slight performance decrease in terms of resonant frequency and bandwidth.

Taking a closer look at Figure 12 shows that OS4 (Optimized System 4) has doubled the extracted peak power from 0.080 Hz to 0.156 Hz, and OS5 (Optimized System 5) has a slight more power in the 0.156 Hz- 0.390 Hz range. This is a clear indication that OS4 is better suited for the Australian sea conditions where the wave frequencies are mostly below 0.156 Hz. Table 7 confirms the findings of Figure 12, even though OS5 has a maximum power of 60.548 kW at a resonant frequency of 0.104 Hz, which makes it well established to function in areas with low frequencies, OS4 has a higher maximum power peak of 106.470 kW (76% increase) at a lower resonant frequency of 0.089 Hz (well within the average of Australian waves' frequencies).

The fourth column of Table 7 represents the bandwidth of the optimized systems. OS4's bandwidth might seem low at 0.048Hz, especially compared to OS 5's 0.193Hz bandwidth, but taking a closer look at the numbers indicate that this range is almost entirely within the range of frequencies of Australian ocean waves. With an upper bound of 0.123 Hz which is very close to the upper bound of Australian ocean waves frequencies (0.125Hz), and a lower bound of 0.075Hz, which means that this bandwidth includes the lower bound of the Australian ocean waves frequencies (0.0833Hz).

Therefore, this section presented an optimization method based on the parametric study outcomes obtained from the Taguchi method, and iterated two derived systems to optimize them for the Australian sea conditions with some sacrifices in maximum power. OS4 is clearly better suited for this project with higher absorbed power in the range of the target locations (low frequency operation) than OS5.

6. Conclusion

This paper identified the problem of the multidisciplinary nature of wave energy converters. A parametric study was conducted to investigate the effect of the system parameters on the wave energy conversion performance of the heaving point absorber with a submerged body based on the Taguchi method.

The parametric study was used to identify the best combination of parameters in a system to deliver the best output performance. The output performance attributes studied were: the maximum absorbed average power, the resonant frequency and the bandwidth of the system. One important aspect looked at was the shape of the submerged body which was altered between a cylinder and a sphere. A cylindrical shape presents excellent hydrodynamic properties with high added mass and radiating capabilities which results in high system inertia and should perform well at low frequencies but it has high viscous damping compared to the spherical shape, which results in a lower absorbed power. Even though the spherical submerged body has less added mass and radiating capabilities, it can capture more power with the low viscous damping. Therefore a study was made to determine the best system in terms of both operational frequency range and captured power.

According to the outcomes of the Taguchi method, it was found that the shape of the submerged body had the largest effect on captured power, followed by the buoy's diameter, submerged body depth and PTO damping. The rest of the parameters had a lower effect on the captured power. The volume of the submerged body had the biggest effect on the resonant frequency, in comparison, the rest of the parameters had a negligible effect on the resonant frequency. Finally, almost all the parameters had an effect on the bandwidth. The submerged body shape and PTO stiffness have the largest effects, and the PTO damping has a negligible effect, this is a good indication of the dependency of all the parameters and how the system parameters affect the upper and lower bounds of the operational range.

Finally, two systems were identified from the Taguchi method, they are System 4 and System 5. System 4 had the maximum captured power peak, and System 5 had the best operational frequencies range. These two systems were further optimized from the findings of Taguchi method in an attempt to capture the maximum power while operating at low frequencies, which are suitable for the Australian ocean waves' state. It was found that OS4 had the best overall performance, and that a two body WEC system with a spherical submerged body should be optimized to present good system inertia and result in good performance at low frequencies, but at the cost of a reduction in the captured power.

The parametric study and optimization method presented in this paper should provide a future guide for two-body WEC designs, and compromises must be made to achieve a good performance at a certain sea state.

ACKNOWLEDGEMENT

Authors would like thank Australia Research Council Discovery Project grant DP170101039 for financial support.

Appendix A

Table 8 : Taguchi method' L8 matrix and outcomes

INPUT VARIABLES								OUTPUT MEASURE:
								NOMINAL (TARGET):
RUN	1	2	3	4	5	6	7	AVERAGE
1	1	1	1	1	1	1	1	43806
2	1	1	1	2	2	2	2	83152
3	1	2	2	1	1	2	2	61432
4	1	2	2	2	2	1	1	245000
5	2	1	2	1	2	1	2	36210
6	2	1	2	2	1	2	1	147620
7	2	2	1	1	2	2	1	21327
8	2	2	1	2	1	1	2	62690
AVERAGE **1**	108,347.50	77,697.00	52,743.75	40,693.75	78,887.00	96,926.50	114,438.25	
2	66,961.75	97,612.25	122,565.50	134,615.50	96,422.25	78,382.75	60,871.00	
EFFECT-	- 41,385.75	19,915.25	69,821.75	93,921.75	17,535.25	-18,543.75	- 53,567.25	
SETTINGS								

Col.	**Variable**	**Level1**	**Level 2**
1 - A	PTO damping	100,000 Ns/m	Variable=External damping
2 - B	PTO Stifness	100,000 kN/m	200,000 kN/m
3	Diameter of buoy	4 m	6 m
4 - C	Submerged body geometry	Sphere	Cylinder
5	Submerged body Volume	33.51 m^3	113.1 m^3
6	Buoy's Draft	1 m	2 m
7	Submerged body depth	20 m	40 m

Appendix B

Table 9: Physical properties of the systems

System	1	2	3	4	5	6	7	8
PTO damping (N.s/m)	100,000	100,000	100,000	100,000	Variable	Variable	Variable	Variable
PTO Stifness (N/m)	100,000	100,000	200,000	200,000	100,000	100,000	200,000	200,000
Buoy's diameter (m)	4	4	6	6	6	6	4	4
Buoy's height (m)	2.5	2.5	2.5	2.5	2.5	2.5	2.5	2.5
Buoy's dry mass (kg)	12906	25811	58075	29038	29038	58075	25811	12906
Buoy's Draft (m)	1	2	2	1	1	2	2	1
Buoy's hydrostatic stiffness (N/m)	126605	126605	284860	284860	284860	284860	126605	126605
Submerged body geometry	Cylinder	Sphere	Cylinder	Sphere	Cylinder	Sphere	Cylinder	Sphere
Submerged body Volume (m^3)	33.51	113.1	33.51	113.1	113.1	33.51	113.1	33.51
Submerged body depth (m)	20	40	40	20	40	20	20	40
Submerged body radius (m)	2	3	2	3	3	2	3	2
Submerged body height (m)	2.667	-	2.667	-	4	-	4	-
Submerged body dry mass (kg)	34415	116154	34415	116154	116154	34415	116154	34415
Simulation water depth (m)	400	400	400	400	400	400	400	400
Water density (kg/m^3)	1027	1027	1027	1027	1027	1027	1027	1027
viscous drag coefficient	1	0.1	1	0.1	1	0.1	1	0.1
Wave height (m)	1	1	1	1	1	1	1	1

References

[1] B. Drew, A.R. Plummer, M.N. Sahinkaya, A review of wave energy converter technology, Proceedings of the Institution of Mechanical Engineers, Part A: Journal of Power and Energy, 223 (2016) 887-902.
[2] A.F.d.O. Falcão, Wave energy utilization: A review of the technologies, Renewable and Sustainable Energy Reviews, 14 (2010) 899-918.
[3] J. Engström, V. Kurupath, J. Isberg, M. Leijon, A resonant two body system for a point absorbing wave energy converter with direct-driven linear generator, Journal of Applied Physics, 110 (2011).
[4] H. Polinder, B.C. Mecrow, A.G. Jack, P.G. Dickinson, M.A. Mueller, Conventional and TFPM Linear Generators for Direct-Drive Wave Energy Conversion, IEEE Transactions on Energy Conversion, 20 (2005) 260-267.
[5] M. Eriksson, J. Isberg, M. Leijon, Hydrodynamic modelling of a direct drive wave energy converter, International Journal of Engineering Science, 43 (2005) 1377-1387.
[6] J.S. Park, B.-G. Gu, J.R. Kim, I.H. Cho, I. Jeong, J. Lee, Active Phase Control for Maximum Power Point Tracking of a Linear Wave Generator, IEEE Transactions on Power Electronics, 32 (2017) 7651-7662.
[7] S.J. Illesinghe, R. Manasseh, R. Dargaville, A. Ooi, Idealized design parameters of Wave Energy Converters in a range of ocean wave climates, International Journal of Marine Energy, 19 (2017) 55-69.
[8] J. Pastor, Y. Liu, Frequency and time domain modeling and power output for a heaving point absorber wave energy converter, International Journal of Energy and Environmental Engineering, 5 (2014).
[9] H.-J. Koh, W.-S. Ruy, I.-H. Cho, H.-M. Kweon, Multi-objective optimum design of a buoy for the resonant-type wave energy converter, Journal of Marine Science and Technology, 20 (2014) 53-63.
[10] G. Giorgi, J.V. Ringwood, Implementation of latching control in a numerical wave tank with regular waves, Journal of Ocean Engineering and Marine Energy, 2 (2016) 211-226.
[11] M.A.a.A. Sarmento, Hydrodynamic Optimization of the Active surface of a Heaving Point Absorber WEC, EWTEC, Uppsala university, Sweden, 2009.
[12] S. Bozzi, A. Miquel, A. Antonini, G. Passoni, R. Archetti, Modeling of a Point Absorber for Energy Conversion in Italian Seas, Energies, 6 (2013) 3033-3051.
[13] S.J. Beatty, M. Hall, B.J. Buckham, P. Wild, B. Bocking, Experimental and numerical comparisons of self-reacting point absorber wave energy converters in regular waves, Ocean Engineering, 104 (2015) 370-386.
[14] C. Liang, L. Zuo, On the dynamics and design of a two-body wave energy converter, Renewable Energy, 101 (2017) 265-274.
[15] J. Engstrom, HYDRODYNAMIC MODELING FOR A POINT ABSORBER WAVE ENERGY CONVERTER, Faculty of Science and Technology, UPPSALA UNIVERSITET, 2011.
[16] A.F. Davis, J. Thomson, T.R. Mundon, B.C. Fabien, Modeling and Analysis of a Multi Degree of Freedom Point Absorber Wave Energy Converter, (2014) V08AT06A046.
[17] B. Wu, X. Wang, X. Diao, W. Peng, Y. Zhang, Response and conversion efficiency of two degrees of freedom wave energy device, Ocean Engineering, 76 (2014) 10-20.

[18] A. Amiri, R. Panahi, S. Radfar, Parametric study of two-body floating-point wave absorber, Journal of Marine Science and Application, 15 (2016) 41-49.
[19] D. Son, V. Belissen, R.W. Yeung, Performance validation and optimization of a dual coaxial-cylinder ocean-wave energy extractor, Renewable Energy, 92 (2016) 192-201.
[20] V. Piscopo, G. Benassai, L. Cozzolino, R. Della Morte, A. Scamardella, A new optimization procedure of heaving point absorber hydrodynamic performances, Ocean Engineering, 116 (2016) 242-259.
[21] R.K. Roy, A primer on the Taguchi method, Society of Manufacturing Engineers, 2010.
[22] J. Morim, N. Cartwright, A. Etemad-Shahidi, D. Strauss, M. Hemer, A review of wave energy estimates for nearshore shelf waters off Australia, International Journal of Marine Energy, 7 (2014) 57-70.
[23] G. Giorgi, J.V. Ringwood, Nonlinear Froude-Krylov and viscous drag representations for wave energy converters in the computation/fidelity continuum, Ocean Engineering, 141 (2017) 164-175.
[24] X. Wang, Analysis of Electromagnetic Vibration Energy Harvesters With Different Interface Circuits, Frequency Analysis of Vibration Energy Harvesting Systems, 2016, pp. 69-106.
[25] C. Siow, J. Koto, H. Abyn, N. Khairuddin, Linearized Morison Drag for Improvement Semi-Submersible Heave Response Prediction by Diffraction Potential, Science and Engineering, 6 (2014).
[26] B. Guo, R. Patton, S. Jin, J. Gilbert, D. Parsons, Non-linear Modelling and Verification of a Heaving Point Absorber for Wave Energy Conversion, IEEE Transactions on Sustainable Energy, (2017) 1-1.
[27] D.C. Montgomery, Design and Analysis of Experiments, John Wiley & Sons, 2008.
[28] P. Alexander, E. Indelicato, A semiempirical approach to a viscously damped oscillating sphere, European Journal of Physics, 26 (2005) 1-10.
[29] B. M.A., B. Aurélien, G. Lionel, F. Pierre, Assessment of Viscous Damping via 3D-CFD Modelling of a Floating Wave Energy Device, 2015.
[30] G.H. Keulegan, L.H. Carpenter, U.S.O.o.N. Research, Forces on Cylinders and Plates in an Oscillating Fluid, U.S. Department of Commerce, National Bureau of Standards, 1956.
[31] E. Achenbach Experiments on the flow past spheres at very high Reynolds numbers, 1972.
[32] J. Falnes, Wave-energy conversion through relative motion between two single-mode oscillating bodies, J Offshore Mech Arct, 121 (1999) 32-38.
[33] A. Babarit, A.H. Clément, Optimal latching control of a wave energy device in regular and irregular waves, Applied Ocean Research, 28 (2006) 77-91.

A parameter study and optimization of two body wave energy converters
Highlights document

- Two-body wave energy converters were parametrically studied using Taguchi method.
- The results form a design guideline of two-body converters.
- The converters with different submerged body shapes are optimized.
- The coupled design parameters and their effects of the converters are identified.

Table 1: Taguchi method L8 matrix

	Parameter 1	Parameter 2	Parameter 3	Parameter 4	Parameter 5	Parameter 6	Parameter 7
System	PTO damping (N.s/m)	PTO Stifness (N/m)	Diameter of buoy (m)	Submerged body geometry	Submerged body Volume (m^3)	Buoy's Draft (m)	Submerged body depth (m)
1	c_p=100000	k_1=100,000	4	Cylinder	33.51	1	20
2	c_p=100000	k_1=100,000	4	Sphere	113.1	2	40
3	c_p=100000	k_2=200,000	6	Cylinder	33.51	2	40
4	c_p=100000	k_2=200,000	6	Sphere	113.1	1	20
5	Variable	k_1=100,000	6	Cylinder	113.1	1	40
6	Variable	k_1=100,000	6	Sphere	33.51	2	20
7	Variable	k_2=200,000	4	Cylinder	113.1	2	20
8	Variable	k_2=200,000	4	Sphere	33.51	1	40

Table 2: Output performance attributes of the 8 systems

System	Max Power (kW)	Resonance frequency (Hz)	Bandwidth (Hz)
1	**43.806**	**0.170**	**0.087**
2	**83.152**	**0.095**	**0.032**
3	**61.432**	**0.192**	**0.059**
4	**245.000**	**0.129**	**0.030**
5	**36.210**	**0.098**	**0.258**
6	**147.620**	**0.174**	**0.028**
7	**21.327**	**0.095**	**0.016**
8	**62.690**	**0.175**	**0.011**

Table 3: Parameter effects on the maximum output power

		Level 1 Power (kW)	Level 2 Power (kW)	Power Effect (kW)	Power Effect (%)
Parameter 1	PTO damping	108.348	66.962	-41.386	44.064
Parameter 2	PTO Stifness	77.697	97.612	19.915	21.204
Parameter 3	Diameter of buoy	52.744	122.566	69.822	74.340
Parameter 4	Submerged body	40.694	134.616	93.922	100.000
Parameter 5	Submerged body Volume	78.887	96.422	17.535	18.670
Parameter 6	Buoy's Draft	96.927	78.383	-18.544	19.744
Parameter 7	Submerged body depth	114.438	60.871	-53.567	57.034

Table 4: Parameter effects on the resonant frequency

		Level 1 resonance frequency (Hz)	Level 2 resonance frequency (Hz)	Frequency Effect (Hz)	Frequency Effect (%)
Parameter 1	PTO damping	0.147	0.136	-0.011	14.97
Parameter 2	PTO Stiffness	0.134	0.148	0.014	18.37
Parameter 3	Diameter of buoy	0.134	0.148	0.015	19.73
Parameter 4	Submerged body	0.139	0.143	0.005	6.12
Parameter 5	Submerged body Volume	0.178	0.104	-0.074	100.00
Parameter 6	Buoy's Draft	0.143	0.139	-0.004	5.44
Parameter 7	Submerged body depth	0.142	0.140	-0.002	2.72

Table 5: Parameter effects on the bandwidth

		Level 1 Bandwidth (Hz)	Level 2 Bandwidth (Hz)	Bandwidth effect (Hz)	Bandwidth effect (%)
Parameter 1	PTO damping	0.052	0.079	0.027	33.563
Parameter 2	PTO Stifness	0.101	0.029	-0.072	90.125
Parameter 3	Diameter of buoy	0.037	0.094	0.057	71.688
Parameter 4	Submerged body	0.105	0.025	-0.080	100.000
Parameter 5	Submerged body Volume	0.046	0.084	0.038	46.938
Parameter 6	Buoy's Draft	0.097	0.034	-0.063	78.375
Parameter 7	Submerged body depth	0.040	0.090	0.050	62.313

Table 6: Performance of the optimized systems

System	Max power (kW)	Resonance Fr (Hz)	Bandwidth (Hz)	Bandwidth @50% max power (Hz)
4 optimized	106.470	0.089	0.048	0.048
5 optimized	60.548	0.104	0.193	0.193

Table 7 : Taguchi method' L8 matrix and outcomes

INPUT VARIABLES								OUTPUT MEASURE: NOMINAL (TARGET):
RUN	1	2	3	4	5	6	7	AVERAGE
1	1	1	1	1	1	1	1	43806
2	1	1	1	2	2	2	2	83152
3	1	2	2	1	1	2	2	61432
4	1	2	2	2	2	1	1	245000
5	2	1	2	1	2	1	2	36210
6	2	1	2	2	1	2	1	147620
7	2	2	1	1	2	2	1	21327
8	2	2	1	2	1	1	2	62690
AVERAGE **1**	108348	77697	52744	40694	78887	96927	114438	
2	66962	97612	122566	134616	96422	78383	60871	
EFFECT-	-41386	19915	69822	93922	17535	-18544	-53567	
SETTINGS								
Col.	**Variable**			**Level1**			**Level 2**	
1 - A	PTO damping			100,000 Ns/m			Variable=External damping	
2 - B	PTO stiffness			100,000 N/m			200,000 N/m	
3	Diameter of buoy			4 m			6 m	
4 - C	Submerged body geometry			Sphere			Cylinder	
5	Submerged body volume			33.51 m^3			113.1 m3	
6	Buoy's draft			1 m			2 m	
7	Submerged body depth			20 m			40 m	

Table 8: Physical properties of the systems

System	1	2	3	4	5	6	7	8
PTO damping (N.s/m)	100,000	100,000	100,000	100,000	Variable	Variable	Variable	Variable
PTO Stifness (N/m)	100,000	100,000	200,000	200,000	100,000	100,000	200,000	200,000
Buoy's diameter (m)	4	4	6	6	6	6	4	4
Buoy's height (m)	2.5	2.5	2.5	2.5	2.5	2.5	2.5	2.5
Buoy's dry mass (kg)	12906	25811	58075	29038	29038	58075	25811	12906
Buoy's Draft (m)	1	2	2	1	1	2	2	1
Buoy's hydrostatic stiffness (N/m)	126605	126605	284860	284860	284860	284860	126605	126605
Submerged body geometry	Cylinder	Sphere	Cylinder	Sphere	Cylinder	Sphere	Cylinder	Sphere
Submerged body Volume (m^3)	33.51	113.1	33.51	113.1	113.1	33.51	113.1	33.51
Submerged body depth (m)	20	40	40	20	40	20	20	40
Submerged body radius (m)	2	3	2	3	3	2	3	2
Submerged body height (m)	2.667	-	2.667	-	4	-	4	-
Submerged body dry mass (kg)	34415	116154	34415	116154	116154	34415	116154	34415
Simulation water depth (m)	400	400	400	400	400	400	400	400
Water density (kg/m^3)	1027	1027	1027	1027	1027	1027	1027	1027
viscous drag coefficient	1	0.1	1	0.1	1	0.1	1	0.1
Wave height (m)	1	1	1	1	1	1	1	1